PERGAMON

Renewable Energy 25 (2002) 341–369

RENEWABLE ENERGY

www.elsevier.nl/locate/renene

Heat transfer coefficient and friction factor correlations for rectangular solar air heater duct having transverse wedge shaped rib roughness on the absorber plate

J.L. Bhagoria [a], J.S. Saini [b,*], S.C. Solanki [b]

[a] *Department of Mechanical Engineering, M.A.C.T. (R.E.C.), Bhopal 462007, India*
[b] *Department of Mechanical and Industrial Engineering, University of Roorkee, Roorkee 247667, India*

Received 15 December 2000; accepted 15 January 2001

Abstract

As is well known, the heat transfer coefficient of a solar air heater duct can be increased by providing artificial roughness on the heated wall (i.e. the absorber plate). Experiments were performed to collect heat transfer and friction data for forced convection flow of air in solar air heater rectangular duct with one broad wall roughened by wedge shaped transverse integral ribs. The experiment encompassed the Reynolds number range from 3000 to 18000; relative roughness height 0.015 to 0.033; the relative roughness pitch $60.17\phi^{-1.0264} < p/e < 12.12$; and rib wedge angle ($\phi$) of 8, 10, 12 and 15°. The effect of parameters on the heat transfer coefficient and friction factor are compared with the result of smooth duct under similar flow conditions. Statistical correlations for the Nusselt number and friction factor have been developed in terms of geometrical parameters of the roughness elements and the flow Reynolds number.

Keywords: Solar air heater; Heat transfer; Friction

1. Introduction

Forced convection heat transfer in smooth and roughened ducts has been investigated by several investigators, and a large amount of useful information is available

* Corresponding author. Fax: +91-1332-65242.
E-mail address: sainifme@rurkiu.ernet.in (J.S. Saini).

0960-1481/02/$ - see front matter
PII: S0960-1481(01)00057-X

Nomenclature

A	area of cross-section, m^2
A_c	surface area of collector, m^2
A_o	throat area of orifice plate, m^2
C_d	coefficient of discharge for orifice meter
c_p	heat of air at constant pressure, kJ/kg K
D_h	equivalent diameter of the air passage, $D_h=4WH/[2(W+H)]$
e	roughness height, m
e/D_h	relative roughness height
f	friction factor
f_r	friction factor in roughened duct, $f_r=2(\delta p)D_h/4\rho L_f V^2$
f_s	friction factor in a smooth passage, $f_s=2(\delta p)D_h/4\rho L_f V^2$
H	height of air channel, m
h	convective heat transfer coefficient, W m^{-2} K^{-1}
k	thermal conductivity of air, W m^{-1} K^{-1}
L	duct length for calculation of friction factor, m
m	mass flow rate of air, kg/s
Nu	Nusselt number
Nu_s	Nusselt number of smooth duct, $Nu_s=hD_h/k$
Nu_r	Nusselt number of rough duct, $Nu_r=hD_h/k$
p	pitch
p/e	relative roughness pitch
δp	pressure drop across the test section, Pa
δp_o	pressure drop across the orifice meter, Pa
q	rate of heat transfer to air, W
Re	Reynolds number, $\rho VD_h/\mu$
$\overline{t_f}$	average temperature of air, K
$\overline{t_p}$	average temperature of plate, K
$\overline{t_i}$	bulk mean temperature of air at inlet, K
$\overline{t_o}$	bulk mean temperature of air at outlet, K
V	velocity of air, m/s
W	width of air duct, m
W/H	channel aspect ratio
X	Length in axial direction from inlet, m

Greek symbols

ϕ	wedge angle, degree
α	rib angle of attack, degree
β	ratio of orifice diameter to pipe diameter
ρ	density of air, kg/m^3

Subscripts

r	roughened duct
s	smooth duct

in the literature. The use of artificial roughness on a surface is an effective technique to enhance heat transfer to fluid flowing in the duct. The application of artificial roughness in the form of fine wires and ribs of different shapes has been recommended to enhance the heat transfer coefficient by several investigators [1–15]. Roughness elements have been used to improve the heat transfer coefficient by creating turbulence in the flow. However, it would also result in an increase in friction losses and hence greater power requirements for pumping air through the duct. In order to keep the friction losses at a low level, the turbulence must be created only in the region very close to the duct surface, i.e. in the laminar sublayer. A number of investigations have been carried out on the heat transfer characteristics of channels or pipes with roughness elements on the surface. Nikuradse [1] investigated the effect of roughness on the friction factor and velocity distribution in pipes roughened by sand blasting. Nunner [2] and Dippery and Sebersky [3] developed a friction similarity law and a heat momentum transfer analogy for flow in sand grain roughened tubes. Ravigururajan and Bergles [4] developed general statistical correlations for heat transfer and pressure drop for four types of roughness, namely semicircular, circular, rectangular and triangular for single-phase turbulent flow in internally ribbed tubes. Han [5] carried out an experimental study in square duct with two opposite rib roughened walls. Webb and Eckert [6] developed the heat transfer and friction factor correlations for turbulent air flow in tubes having rectangular repeated rib roughness. Han and Zhang [7] investigated the effect of parallel and V-shaped broken rib orientation on the local heat transfer distribution and pressure drop in a square channel with two opposite ribbed walls. Liou and Hwang [8] investigated experimentally the turbulent heat transfer and friction in a channel with different ridge shapes, namely triangular, semicircular and square ribs mounted on two opposite walls. Most of the investigations carried out so far have been on two opposite roughened walls and with all the four walls heated. It needs to be mentioned that for the application of this concept of enhancement of heat transfer in the case of solar air heaters which in general have low thermal efficiency due to a low convective heat transfer coefficient between the heated absorber plate and the carrier fluid (air), roughness elements have to be considered only on one wall which is the only heated wall. This application makes the fluid flow and heat transfer characteristics distinctly different from those found in the case of two roughened walls and four heated wall ducts. In solar air heaters, only one wall of the rectangular air flow passage is subjected to uniform heat flux (insolation) while the remaining three walls are insulated. Prasad and Saini [9] investigated heat transfer and the friction factor in a solar air heater

using transverse rib on the absorber plate. The roughened wall was prepared by gluing thin copper wires. Gupta et al. [10] carried out an experimental study in a solar air heater duct with non-transverse ribs on the absorber plate. Saini and Saini [11] used expanded metal matrix roughness on the heated wall while Karwa et al. [12] experimented on integral chamfered rib roughness on the heated wall.

As mentioned above a variety of roughness geometries have been used as artificial roughness to enhance the heat transfer rate. Most of these ribs are attached to the heat transfer surface by gluing, resulting in large contact resistance and this reduces the effective area of the heat transfer. This problem of high contact resistance could be solved by the use of integral ribs. The other important consideration is the substantial increase in the friction losses and corresponding pumping power requirements. It has been found that the chamfered and wedge shaped ribs have relatively lower enhancement of this penalty [13]. Williams et al. [13] reported the results in the form of Stanton number, friction factor and thermal performance by using different types of transverse roughness elements, namely rectangular, chamfered, wedge and helical ribs on a circular annulus flow passage. They found the optimum angle for chamfer ribs, wedge ribs and helical ribs and the thermal performance at different angles with a pitch/height of about 7 and Reynolds number of 8×10^5. The results showed that the thermal performance of wedge ribs is superior to that of chamfer and helical ribs. Thus, the application of such ribs to a solar air heater is worth exploring.

The objective of the present investigation is to generate friction and heat transfer data pertinent to the heating of air in a rectangular duct with wedge shaped transverse repeated rib roughness on one broad heated wall. The statistical correlations for Nusselt number and friction factor in terms of roughness parameters have been developed, and the effect of system and operating parameters on the performance have been discussed.

2. Roughness geometry and range of parameters

Table 1 gives the range of roughness and flow parameters covered in the present study. Figure 1(a, b, c) shows the general geometry of the ribbed section. It can be seen that the cross-section of rib is determined by the values of angle, ϕ (or vertex angle, $90-\phi$) and the rib height, e. The limiting case of the pitch (lowest pitch) is indicated in Fig. 1(b) where the toe of one rib touches the front bottom edge of the next rib. In such a case the relative roughness pitch (p/e) can be proved to be given

Table 1
Range of parameters

Reynolds number, *Re*	3000–18000
Relative roughness height, e/D_h	0.015–0.033
Relative roughness pitch, p/e	$60.17\phi^{-1.0264}<p/e<12.12$
Rib wedge angle, ϕ	8°–15°
Aspect ratio of duct, W/H	5

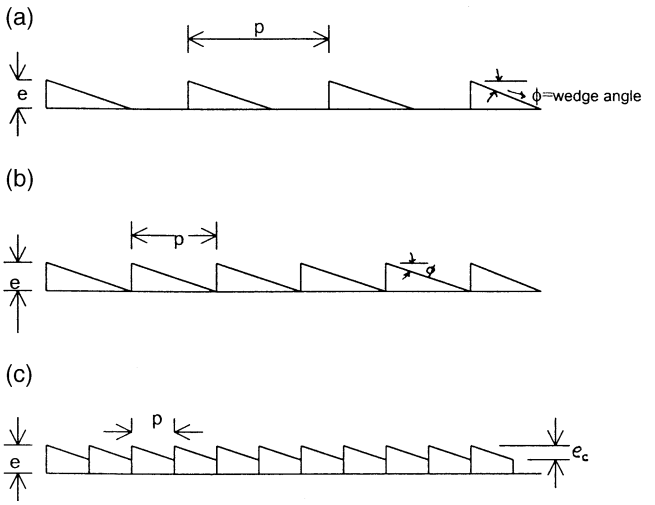

Fig. 1. Rib geometries.

by $p/e=60.17\phi^{-1.0264}$. This is the case of the lowest pitch because any pitch value below this will be a case equivalent to a limiting case of another pitch ratio as can be explained in Fig. 1(c).

The case shown in Fig. 1(c) is equivalent, from the fluid dynamics point of view, to a case of limiting pitch ratio of p/e_c (here $p/e_c=60.17\phi^{-1.0264}$) although this ribbed surface has been prepared to represent a pitch "p" and height "e". Here $p/e<p/e_c$ or $p/e<60.17\phi^{-1.0264}$. In view of this, the range of relative roughness pitch has been selected and represented as $60.17\phi^{-1.0264}<p/e<12.12$.

Table 2 gives the dimensions of roughened plates. Twenty wedge shaped ribs of varying geometries have been used for study in addition to a smooth duct for which data under similar operating conditions have been collected for the purpose of comparison with roughened ducts.

3. Experimental program

3.1. Experimental set-up

A schematic diagram of the experimental set-up including the test section is shown in Fig. 2. The flow system consists of an entry section, a test section, an exit section, a flow meter and a centrifugal blower. The duct is of size 2600 mm×150 mm×30 mm (dimension of inner cross-section) and is constructed from wooden panels of 25 mm thickness. The test section is of length 1640 mm (32.8 D_h). The entry and exit lengths were 360 mm (7.2 D_h) and 600 mm (12 D_h), respectively. A short entrance length ($L/D_h=7.2$) was chosen because for a roughened duct the thermally fully developed flow is established in a short length 2–3 hydraulic diameter [14,15].

Table 2
Dimensions of roughened plates: Angle of attack, α=90°

Plate No.	Rib height e (mm)	Pitch p (mm)	Wedge angle ϕ (°)	p/e	e/D_h
1	1.65	11.74	8	7.11	0.033
2	1.65	12.50	8	7.57	0.033
3	1.65	16.50	8	10	0.033
4	1.65	20.00	8	12.12	0.033
5	1.65	9.35	10	5.67	0.033
6	1.65	12.50	10	7.57	0.033
7	1.65	16.50	10	10.0	0.03
8	1.65	20.00	10	12.12	0.033
9	1.65	7.76	12	4.7	0.033
10	1.65	12.50	12	7.57	0.033
11	1.65	16.50	12	10.0	0.033
12	1.65	20.00	12	12.12	0.033
13	1.65	6.15	15	3.73	0.033
14	1.65	12.50	15	7.57	0.033
15	1.65	16.50	15	10.0	0.033
16	1.65	20.00	15	12.12	0.033
17	1.40	10.60	10	7.57	0.028
18	1.25	9.45	10	7.57	0.025
19	1.00	7.57	10	7.57	0.02
20	0.75	5.68	10	7.57	0.015

For the turbulent flow regime, ASHRAE standard 93–77 [16] recommends entry and exit length of $5\sqrt{WH}$ and $2.5\sqrt{WH}$, respectively. The exit section of 600 mm (12 D_h) length is used after the test section in order to reduce the end effect in the test section. In the exit section after 200 mm, three equally spaced baffles are provided in a 100 mm length for the purpose of mixing the hot air coming out of solar air duct to obtain a uniform temperature of air (bulk mean temperature) at the outlet. An electric heater having a size of 1650 mm×150 mm was fabricated by combining series and parallel loops of heating wire on 5 mm asbestos sheet. A mica sheet of 1 mm is placed between the electric heater and absorber plate. This mica sheet acts as an insulator between the electric heater and absorber plate (aluminium plate). The heat flux may be varied from 0 to 1000 W/m^2 by a variac across it. The back of the heater is covered by a 50 mm glasswool layer and a 12 mm thick plate of wood to insulate the top of the heater assembly. The outside of the entire set-up, from the inlet to the orifice plate, is insulated with 25 mm thick polystyrene foam having a thermal conductivity of 0.037 Wm^{-1}K^{-1}. The heated plate is a 6 mm thick aluminium plate with integral rib-roughness formed on its rear side and this forms the top broad wall of the duct, while the bottom wall is formed by 1 mm aluminium plate and 25 mm wood with insulation below it as shown in Fig. 4. The top side of the entry and exit sections of the duct are covered with smooth faced 8 mm thick plywood. The mass flow rate of air is measured by means of a calibrated orifice meter connected with an inclined manometer, and the flow is controlled by the con-

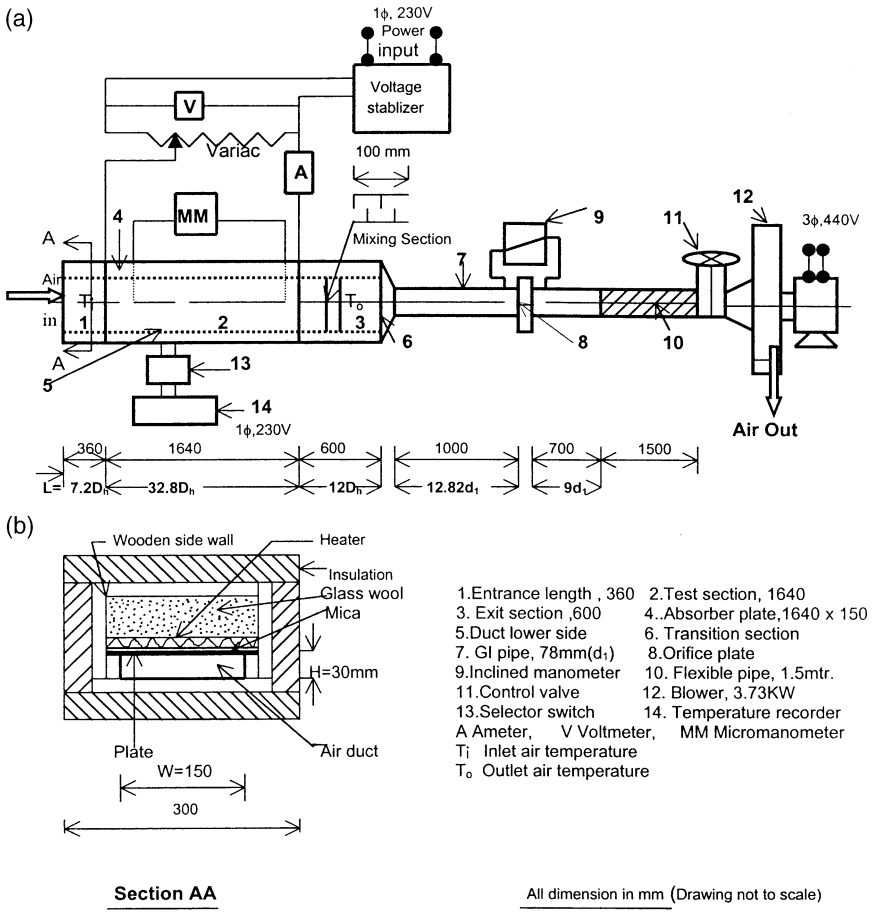

Fig. 2. Schematic diagram of experimental set-up.

trol valves provided in the lines. The orifice plate has been designed for the flow measurement in the pipe of inner diameter of 78 mm, as per the recommendation of Preobrazhensky [17]. The orifice plate is fitted between the flanges, so aligned that it remains concentric with the pipe. The length of the circular GI pipe provided was based on pipe diameter d_1, which is a minimum of 10 d_1 on the upstream side and 5 d_1 on the downstream side of the orifice plate as recommended by Ehlinger [18]. In the present experimental set-up we used 1000 mm (13 d_1) pipe length on the upstream side and 700 mm (9 d_1) on the downstream side. The calibrated copper–constantan 0.3 mm (24 SWG) thermocouples were used to measure the air and the heated plate temperatures at different locations.The location of thermocouples on the heated wall is shown in Fig. 3. A digital micro-voltmeter is used to indicate the output of the thermocouples in °C. The temperature measurement system is calibrated to yield temperature values (t±0.1)°C. The pressure drop across the test section was measured by a micro-manometer.

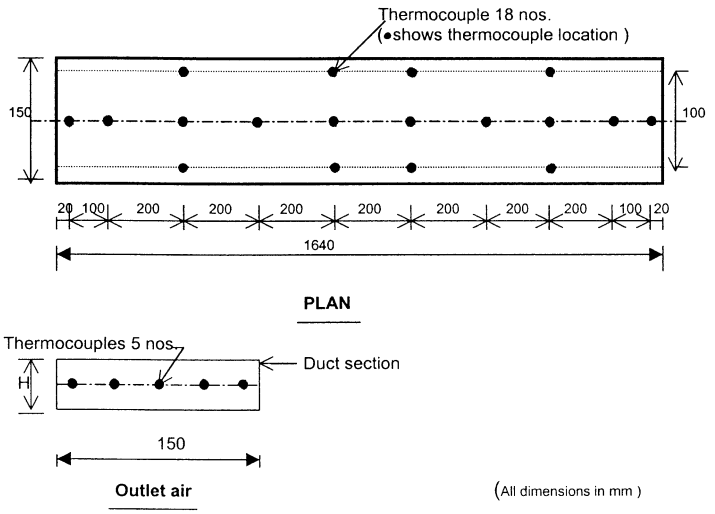

Fig. 3. Location of thermocouples on the absorber plate.

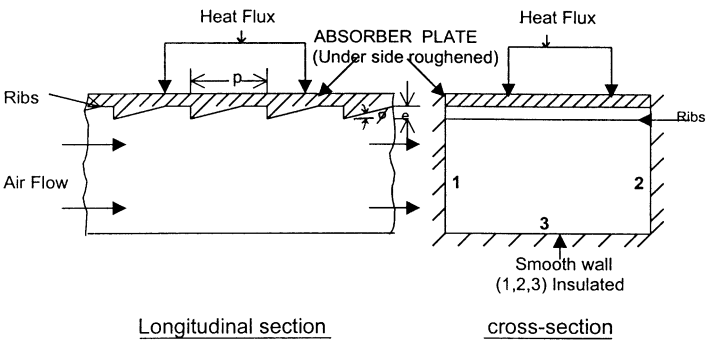

Fig. 4. Duct section with roughness.

3.2. Experimental procedure

The test runs to collect relevant heat transfer and flow friction data were conducted under quasi-steady state conditions. The quasi-steady state condition is assumed to have been reached when the temperature at a point does not change for about 10–12 minutes. When a change in the operating conditions is made, it takes about 20–30 minutes to reach such a quasi-steady state. Eight values of flow rates were used for each set at a fixed heat flux of test [19]. After each change of flow rate, the system was allowed to attain a steady state before the data were recorded. The following parameters were measured:

1. Temperature of the heated plate and temperatures of air at inlet and outlet of the test section

2. Pressure drop across the test section
3. Pressure difference across orifice meter

4. Data reduction

Steady state values of the plate and air temperatures in the duct at various locations were used to determine the values of useful parameters. Mass flow rate, m, heat supplied to the air, q, heat transfer coefficient, h, was calculated as:

$$m = C_d A_o \left[\frac{2\rho(\delta\rho)_o}{1-\beta^4} \right]^{0.5} \tag{1}$$

$$q = mc_p(\bar{t}_o - \bar{t}_i) \tag{2}$$

$$h = \frac{q}{A_c(\bar{t}_p - \bar{t}_f)} \tag{3}$$

where the temperature $\bar{t}_p$ and $\bar{t}_f$ are average values of absorber plate and fluid temperature, respectively. The average value of plate temperature ($\bar{t}_p$) was determined from the detailed temperature profile of the absorbing plate. The plate temperature was determined at eighteen locations on the plate as shown in Fig. 3. The typical variations of plate and air temperatures along the length of the duct were as shown in Fig. 7.

The convective heat transfer coefficient was then used to obtain the average Nusselt number

$$Nu = \frac{hD_h}{k} \tag{4}$$

The friction factor was determined from the measured values of pressure drop, δp, across the test section length, L_f, of 1.2 m (between the two points at 400 mm and 1600 mm from the inlet) as:

$$f = \frac{2(\delta p)D_h}{4\rho L_f V^2} \tag{5}$$

It may be noted that prior to actual data collection, the test setup was checked by conducting experiments for a smooth duct. The Nusselt number and friction factor determined from these experimental data were compared with the values obtained from correlations of the Dittus Boelter equation for the Nusselt number [20] and modified Blasius equation for the friction factor [21]. The results are shown in Fig. 5 and Fig. 6. The friction factor for a smooth rectangular duct is given by the Modified Blasius equation [6] given below:

$$f_s = 0.085Re^{-0.25} \tag{6}$$

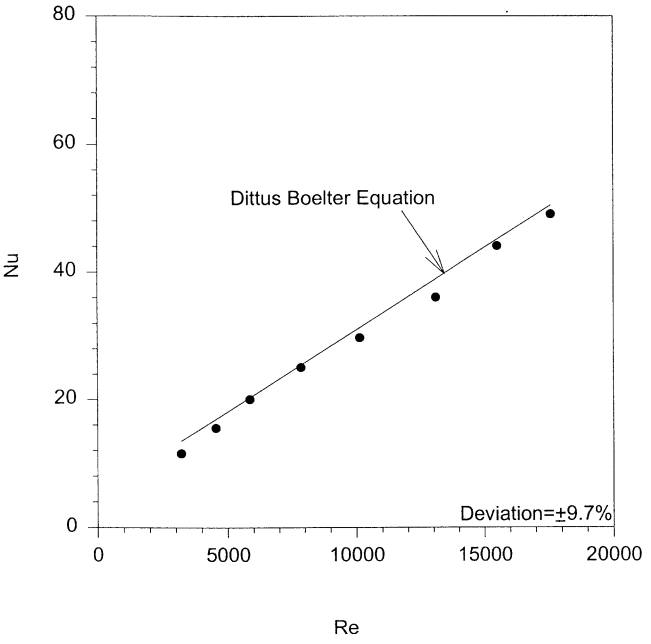

Fig. 5. Nusselt number vs Reynolds number for smooth duct.

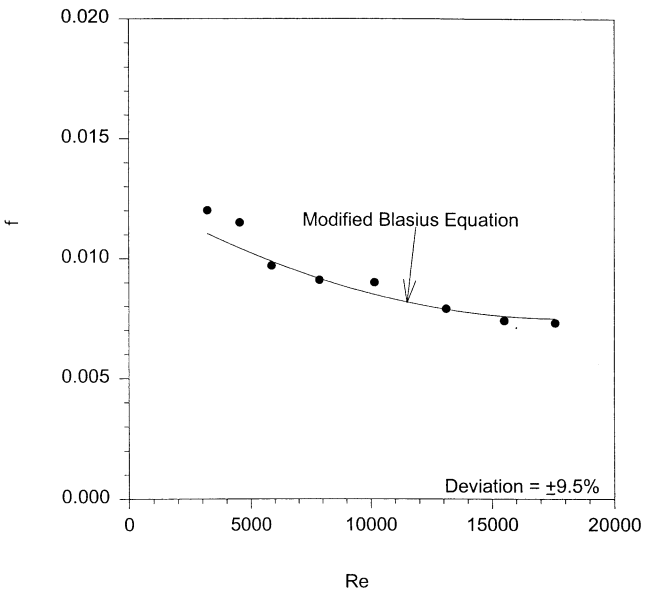

Fig. 6. Friction factor vs Reynolds number for smooth duct.

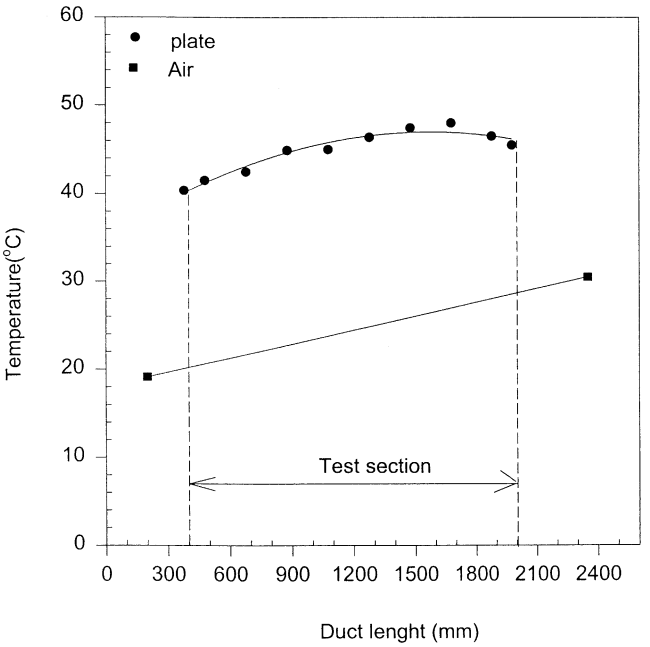

Fig. 7. Plate and air temperature variations in the duct length.

The Nusselt number for a smooth rectangular duct is given by the Dittus and Boelter equation [7] given below:

$$Nu = 0.024 Re^{0.8} Pr^{0.4} \tag{7}$$

The deviation of the present experimental friction data is ±9.5% from the values predicted by Eq. (6). The maximum deviation of Nusselt number data is ±9.7% from the value predicted from Eq. (7), and the experimental values of the friction factor and Nusselt number ensures the accuracy of the experimental data collected with the present set-up. From the analysis of the uncertainties in the measurement by various instruments [22], the maximum uncertainties in the calculated values of various parameters are given below.

Reynolds number=±5.2% (odds of 20:1)
Nusselt number=±5.4% (odds of 20:1)
Friction factor=±7.5% (odds of 20:1)

5. Results and discussion

Figure 8(a and b) show the variations of Nusselt number and friction factor with Reynolds number with the transverse wedge ribs having fixed values of relative

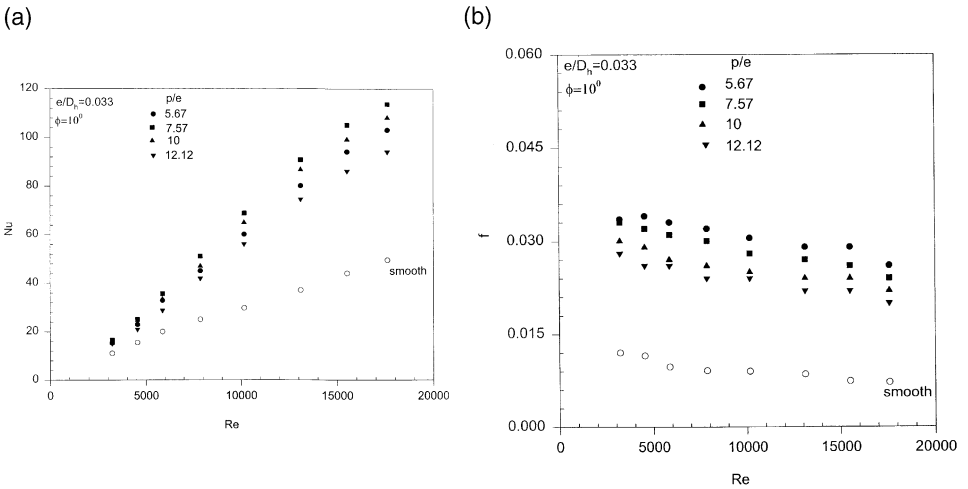

Fig. 8. (a) Nusselt number as a function of Reynolds number for different values of p/e and for fixed e/D_h and ϕ=10°. (b) Friction factor as a function of Reynolds number for different values of p/e and for fixed e/D_h and ϕ=10°.

roughness height and wedge angle, while the relative roughness pitch was varied. It can be seen that the Nusselt number values increase with the increase of Reynolds number, whereas the friction factor decreases with the increase of Reynolds number. It can also be seen from these figures that the enhancement in heat transfer of the roughened duct with respect to the smooth duct also increases with an increase in Reynolds number.

Figure 8(a) shows that the Nusselt number decreases with increasing values of the relative roughness pitch from 7.57 to 12.12. Figure 8(b) also shows a decrease in friction factor with increasing pitch ratio values.

Figures 9 and 10 show the plots of Nusselt number and friction factor, as a function of relative roughness pitch (p/e) for a fixed value of relative roughness height and wedge angle. It is seen that the Nusselt number increases, attains maxima for relative roughness pitch of about 7.57 and then decreases with an increase of relative roughness pitch, whereas friction factor monotonously decreases as the relative roughness pitch increases. It is observed from Fig. 9 that the variation of Nusselt number with relative roughness pitch is insignificant at lower values of Reynolds number, but at higher Reynolds number there is a substantial effect. The variation of Nusselt number with relative roughness pitch of wedge transverse ribs is found to be in the line with the observation of Webb et al. [6], who reported that the separation occurs at the rib, forming a widening free shear layer which reattaches 6–8 rib heights downstream from the separation point. The maximum heat transfer coefficient occurs in the vicinity of the reattachment point [23,24]. Fluid flow pattern for three different pitch values for fixed rib height are shown in Fig. 11(a, b, c). The flow at higher pitch in Fig. 11(a) and (b) reattaches as shown, whereas for low pitch, Fig. 11(c), it may not have reattachment at all. The accelerated and decelerated regions tend to have small

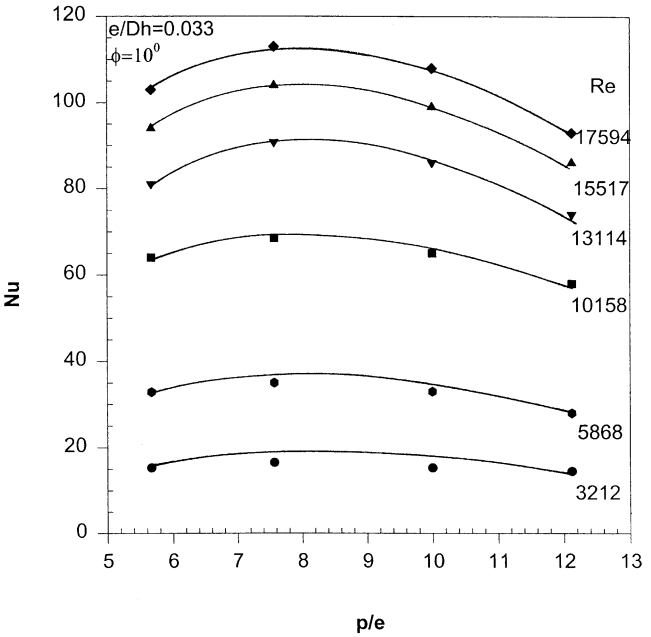

Fig. 9. Nusselt number vs relative roughness pitch.

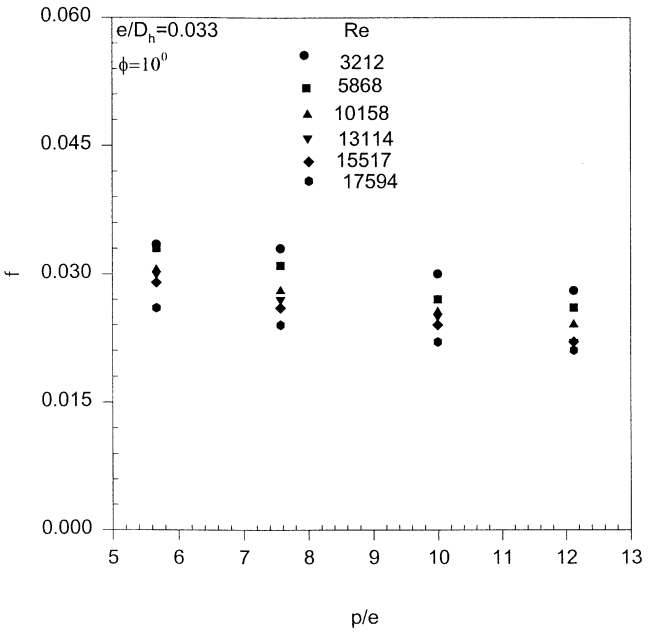

Fig. 10. Friction factor vs relative roughness pitch.

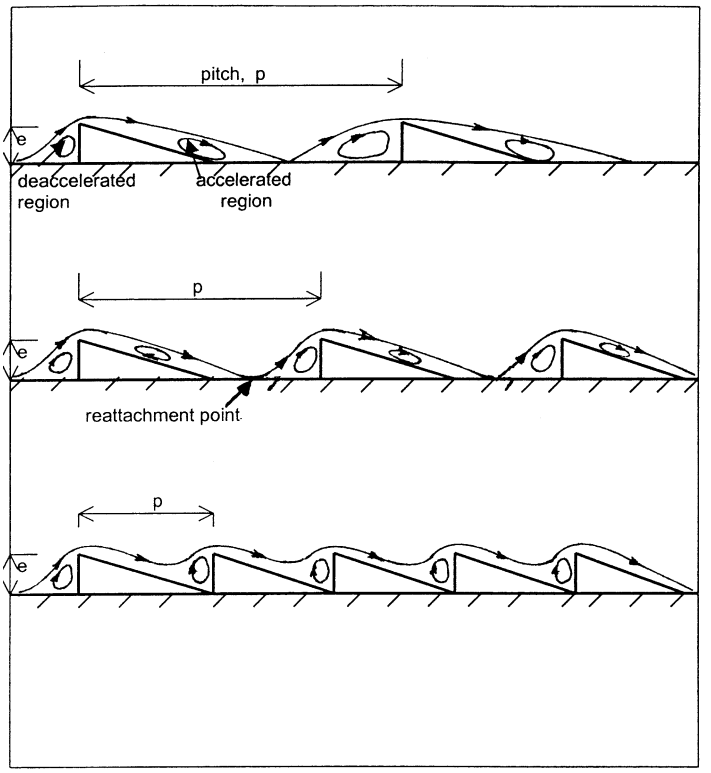

Fig. 11. Approximate model of flow patterns for different pitches.

clockwise rotating eddies as shown in Fig. 11. Flow separated by the rib gets reattached at a position sufficiently before the next rib in Fig. 11(b) where the reattachment point is very close to the next rib. This means that the number of reattachment points is more in comparison to the previous case, Fig. 11(a), for the same length of the base wall. In Fig. 11(c) the flow is not reattached at all because of lower pitch. This would result in a considerable decrease in rate of heat transfer. These observation are confirmed by the experimental results concerning the variation of Nusselt number with pitch.

The variation of Nusselt number and friction factor with relative roughness height have been plotted, respectively, in Fig. 12 and Fig. 13. These figures show a monotonic rise in the values of Nusselt number and friction factor with an increase in the relative roughness height, for given values of flow and roughness parameters. It can be seen that for a higher value of relative roughness height the enhancement in heat transfer is higher at higher Reynolds number values. Similar variation is reported by Prasad and Saini [9]. The maximum enhancement in Nusselt Number and friction factor values are of the order of 2.4 and 2.8, respectively, in the range of experimentation. Flow patterns for different rib height values, keeping wedge angle and relative roughness pitch fixed, are shown in Fig. 14(a, b, c). It can be seen in Fig. 14(a) that

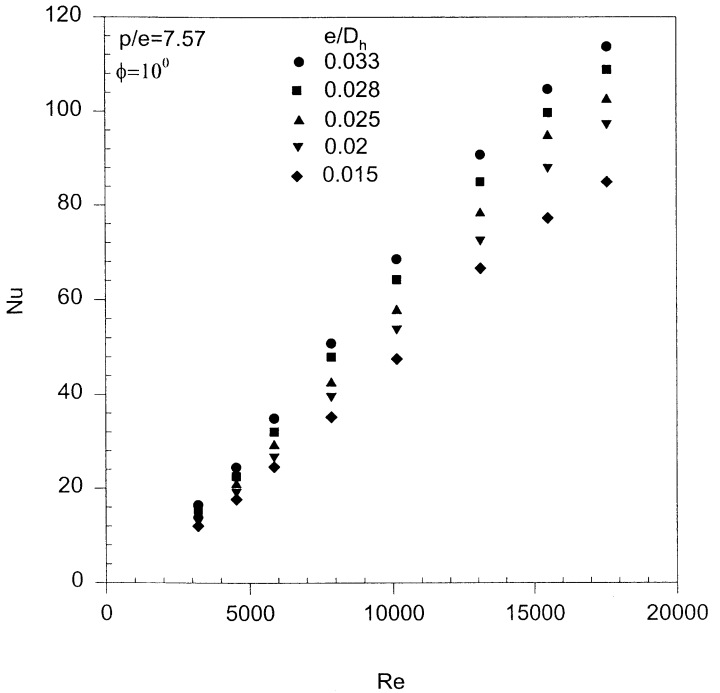

Fig. 12. Nusselt number as a function of Reynolds number for different values of e/D_h and for fixed p/e=7.57 and ϕ=10°.

ribs of smaller height remain submerged in the laminar sublayer, so the flow is likely to be similar both for smooth and roughened duct. This corresponds to a hydraulically smooth flow regime. For a rib height of the order of laminar sublayer, the friction factor will depend upon both the Reynolds number and relative roughness height, and noticeable increase in heat transfer takes place. If the roughness is such that it disturbs the region up to the transition zone without protruding into the turbulent core as shown in Fig. 14(c), friction losses will be very high and the intended purpose will not be served because it disturbs the turbulent core leading to considerably higher friction loss without a corresponding enhancement of heat transfer.

Figures 15 and 16 show the effect of the wedge angle on the Nusselt number and friction factor, respectively. It can be seen from Fig. 15 that the Nusselt number first increases, attains a maximum value at 10° and then sharply decreases with increasing wedge angle, the effect being more pronounced at higher Reynolds number values. It can be seen from Fig. 16 that the friction factor value increases with an increase in wedge angle. Similarly, Figs 17–20 have been drawn to represent the Nusselt number and friction factor as a function of wedge angle for other fixed values of relative roughness pitch. For all the relative roughness pitch ratios, the maxima of Nusselt number occurs nearly for a wedge angle of 10°. The variation of heat transfer coefficient and friction factor with wedge angle is in line with the observation of Williams et al. [13], who reported the results (of different types of transverse ribs,

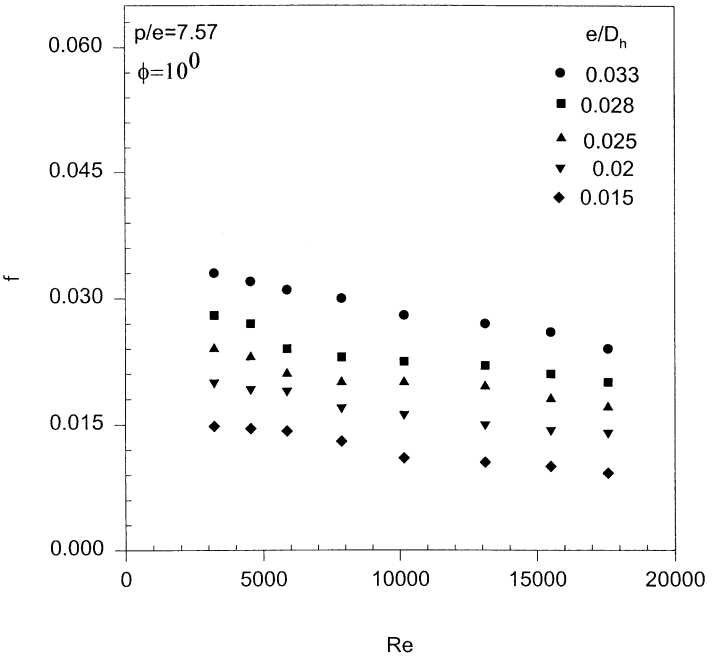

Fig. 13. Friction factor as a function of Reynolds number for different values of e/D_h and for fixed p/e=7.57 and ϕ=10°.

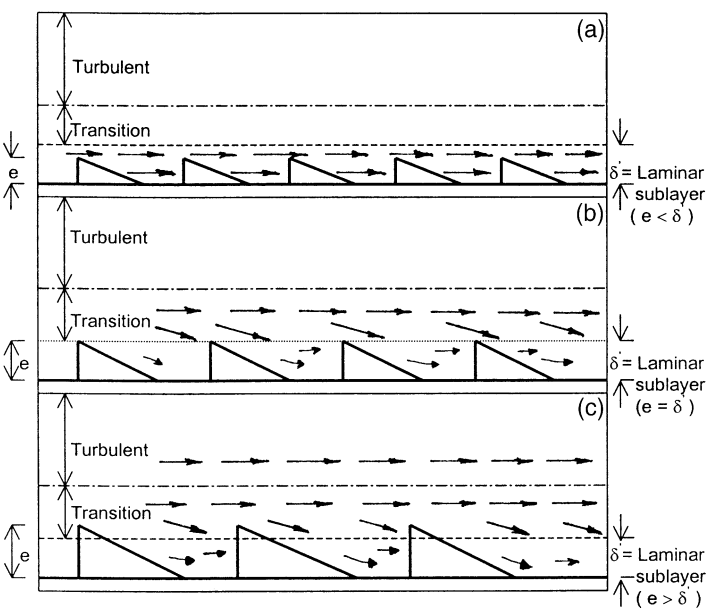

Fig. 14. Approximate model of flow patterns for different rib heights.

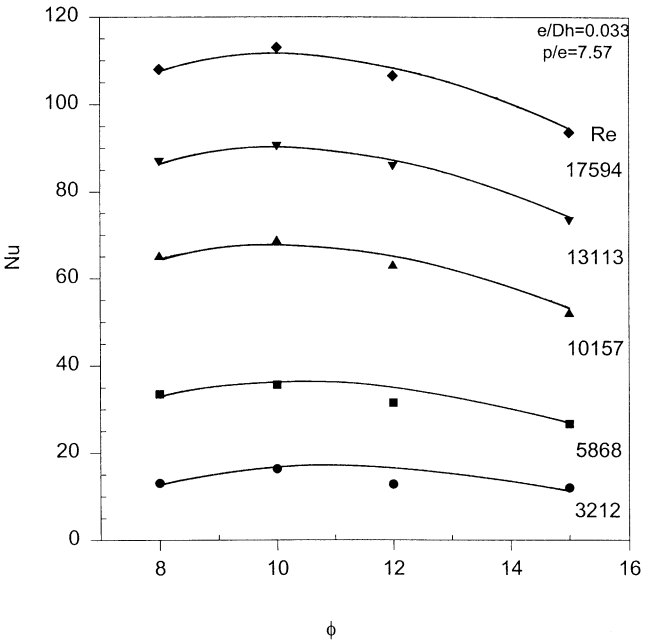

Fig. 15. Nusselt number vs wedge angle for fixed p/e=7.57 and e/D_h=0.033.

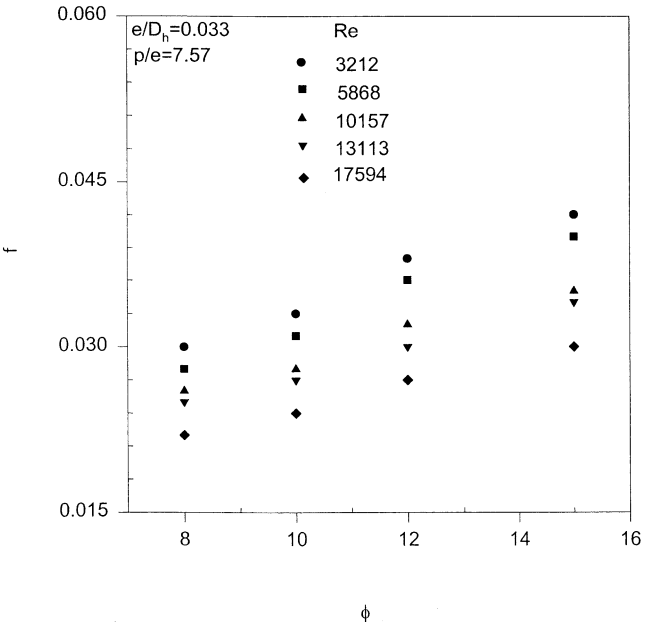

Fig. 16. Friction factor vs wedge angle for fixed p/e=7.57 and e/D_h=0.033.

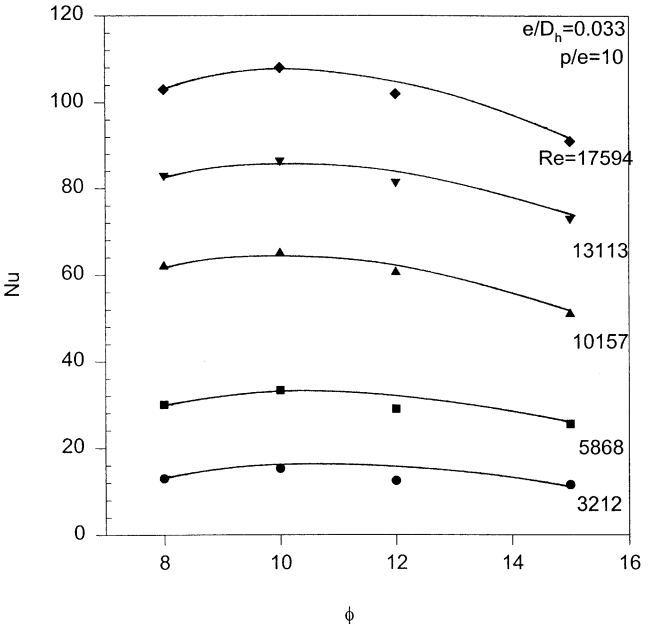

Fig. 17. Nusselt number vs wedge angle for fixed p/e=10 and e/D_h=0.033.

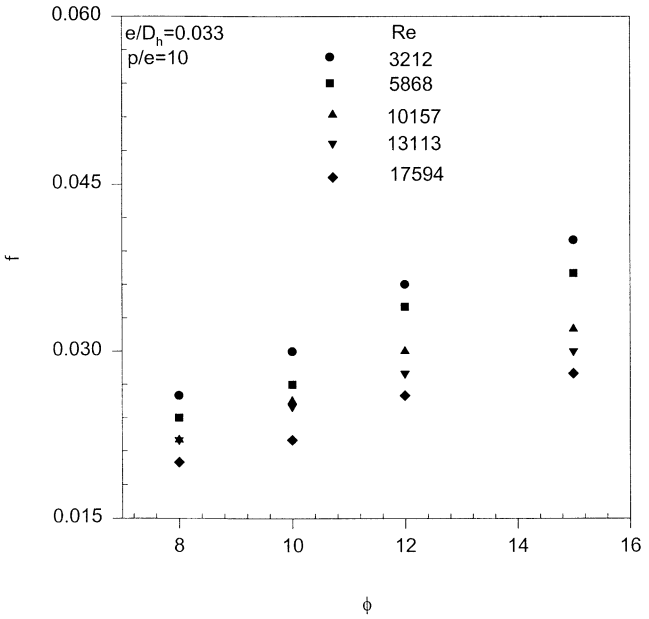

Fig. 18. Friction factor vs wedge angle for fixed p/e=10 and e/D_h=0.033.

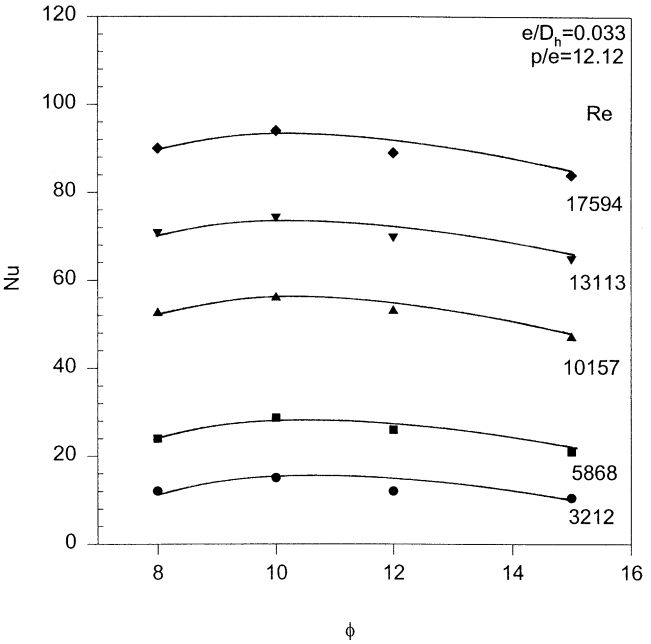

Fig. 19. Nusselt number vs wedge angle for fixed p/e=12.12 and e/D_h=0.033.

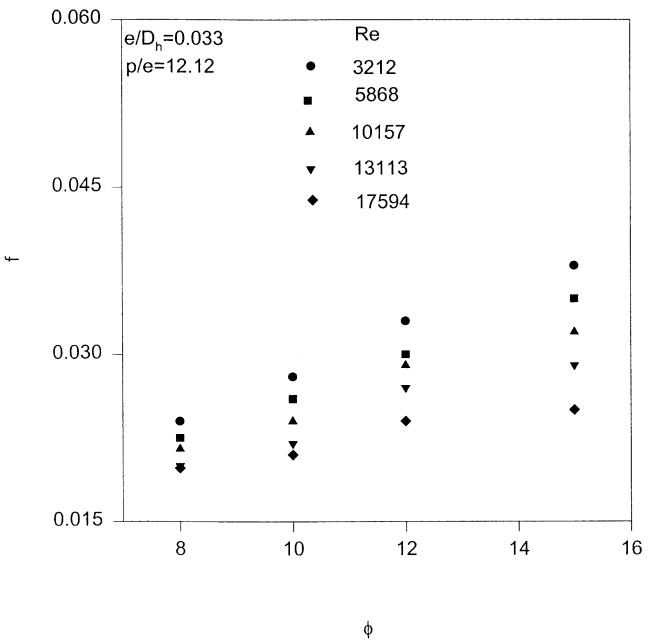

Fig. 20. Friction factor vs wedge angle for fixed p/e=12.12 and e/D_h=0.033.

namely chamfer rib, wedge rib and helical rib) in the form of Stanton number, friction factor and thermal performance ratio, the results showing substantial enhancement in thermal performance of wedge transverse ribs. Figure 21(a, b, c) shows the flow pattern for different shapes of rib geometry. In the case of square and chamfered ribs as seen in Fig. 21(a) and (b) eddies are generated on both sides of the ribs which reduce the heat transfer. The wedge transverse ribs have relatively lesser chance of forming such eddies behind the ribs and this leads to a substantially larger enhancement of heat transfer rate.

6. Correlations for Nusselt number and friction factor

It is evident that designers need a wide ranging correlation that can be used to predict thermal–hydraulic performance or to determine optimum geometric parameters for a particular application. For the results to be useful to designers, statistical correlations are presented here which cover all combinations of the geometric and the flow parameters within the range given in Table 2. As discussed above, Nusselt number and friction factor are strong functions of the geometric and the flow parameters.

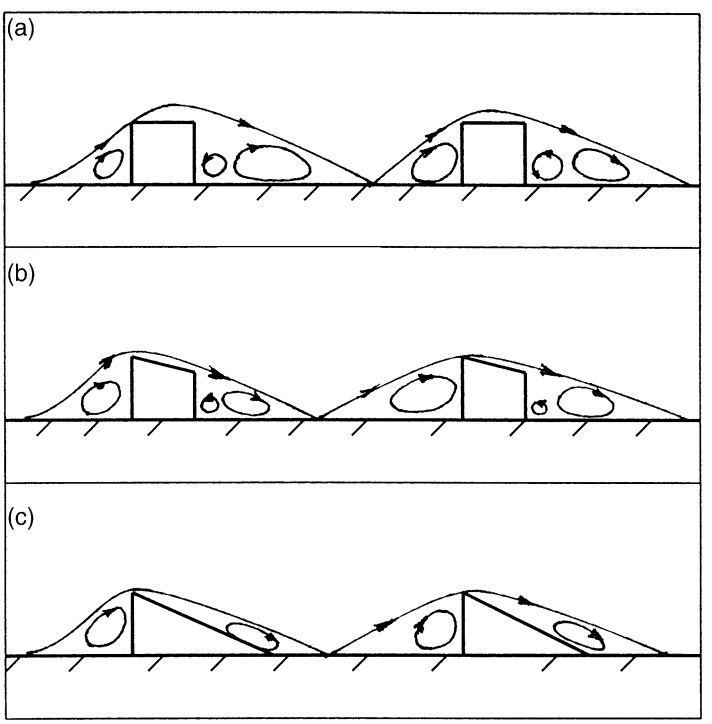

Fig. 21. Approximate model of flow patterns for different geometry (shapes). (a) Square ribs; (b) chamfer ribs; and (c) wedge ribs.

The functional relationship for Nusselt number and friction factor can therefore be written as:

$$Nu_r = f_n(Re, e/D_h, p/e, \phi) \quad (8)$$

$$f_r = f_n(Re, e/D_h, p/e, \phi) \quad (9)$$

7. Correlation for Nusselt number

The experimental data corresponding to all the twenty seven roughened plates (in all, 160 data points) were used for regression analysis to find a relationship that yields a best fit equation for Nusselt number.

Figure 22 shows the Nusselt number as a function of Reynolds number. A regression analysis to fit a straight line on a log–log graph through the data points yields the following power law relation between Nusselt number and Reynolds number:

$$Nu_r = A_0(Re)^{1.21} \quad (10)$$

The coefficient A_0 will in fact be a function of other influencing parameters. Now, taking the parameter relative roughness height of rib (e/D_h) into consideration, the value of $(Nu_r/(Re)^{1.21}=(A_0)$ corresponding to all values of e/D_h are plotted against

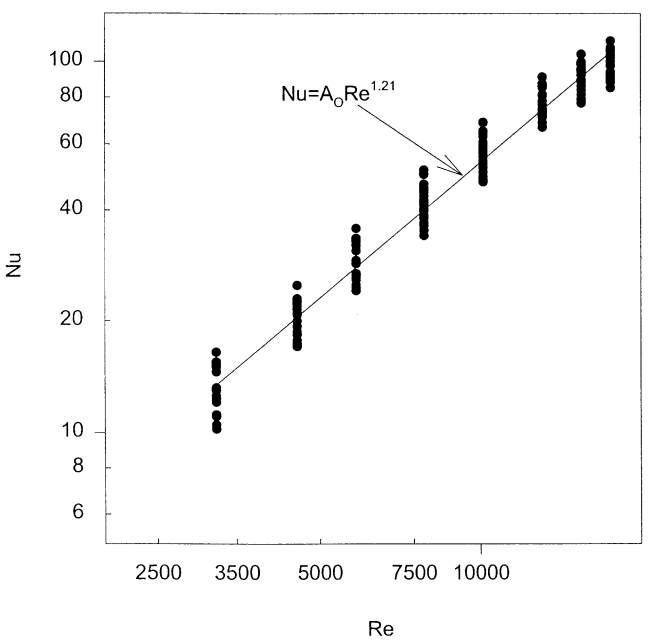

Fig. 22. Plot of *Nu* vs *Re*.

(e/D_h), as shown in Fig. 23. Regression analysis to fit a straight line on a log–log scale through points yields:

$$\frac{Nu}{(Re)^{1.21}} = B_0(e/D_h)^{0.426} \tag{11}$$

Such a relationship was indicated by plots of Nusselt number as a function of relative roughness height of rib (e/D_h), each plot being for given values of flow and all other roughness parameters. Hence B_0 is a function of other influencing parameters. Now considering the parameter relative roughness pitch (p/e), the value of

$$\frac{Nu_r}{(Re)^{1.21}(e/D_h)^{0.426}} (= B_0)$$

has been plotted against (p/e) in Fig. 24. From the regression to fit a second-order quadratic, one obtains

$$\log\left(\frac{Nu_r}{(Re)^{1.21}(e/D_h)^{0.426}}\right) = \log C_0 + C_1(\log(p/e)) + C_2(\log(p/e))^2$$

This Equation can be rearranged as:

$$\frac{Nu_r}{(Re)^{1.21}(e/D_h)^{0.426}} = C_0(p/e)^{2.94}[\exp(-0.71(\ln(p/e))^2)] \tag{12}$$

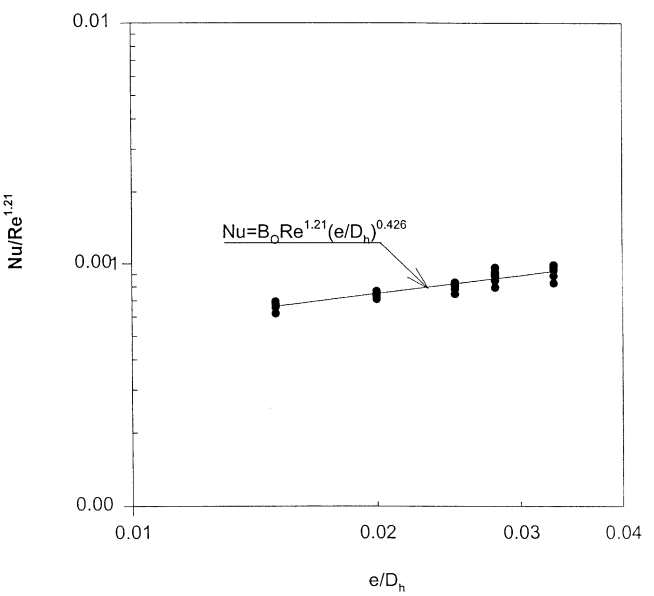

Fig. 23. Plot of $Nu/Re^{1.21}$ vs e/D_h.

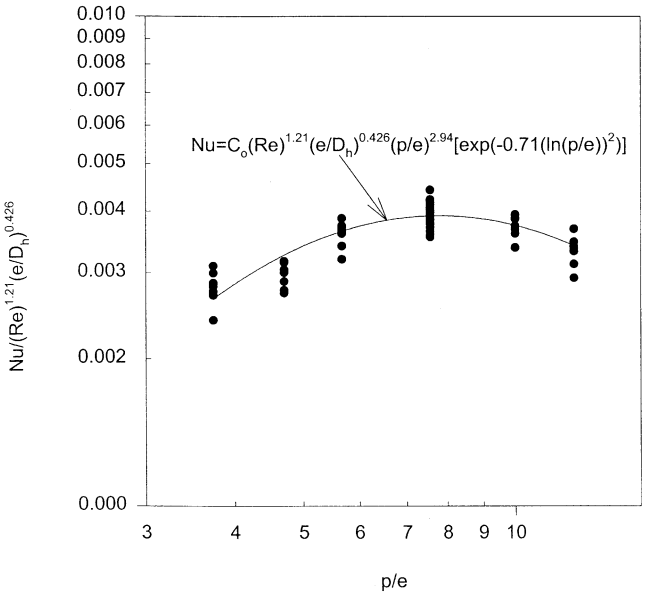

Fig. 24. Plot of $Nu/(Re)^{1.21}(e/D_h)^{0.426}$ vs p/e.

where C_0 is a function of parameter $\phi/10$. Here the normalizing angle of 10° represents the point of maximum enhancement in Nusselt number.

Finally a plot of

$$\frac{Nu_r}{(Re)^{1.21}(e/D_h)^{0.426}(p/e)^{2.94}[\exp(-0.71(\ln(p/e))^2)]}(=C_0)$$

as a function of parameter $\phi/10$, shown in Fig. 25 has been used to fit a second-order quadratic, one obtains

$$\log\left(\frac{Nu_r}{(Re)^{1.21}(e/D_h)^{0.426}(p/e)^{2.94}[\exp(-0.71(\ln(p/e))^2)]}\right)=\log D_0+D_1\log(\phi/10)+D_2(\log(\phi/10))^2$$

This equation can be rearranged as

$$\frac{Nu_r}{(Re)^{1.21}(e/D_h)^{0.426}(p/e)^{2.94}[\exp(-0.71(\ln(p/e))^2)]}=D_0(\phi/10)^{-0.018}[\exp(-1.50(\ln(\phi/10))^2)] \quad (13)$$

The values of the coefficients are:

$A_0=7.46\times10^{-4}$, $B^0=3.9\times10^{-3}$, $C_0=1.9\times10^{-4}$, $D_0=1.89\times10^{-4}$.

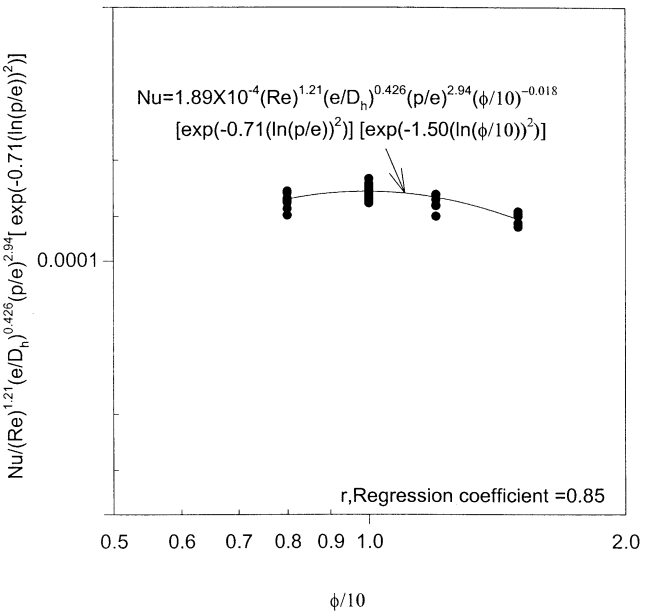

Fig. 25. Plot of $Nu/(Re)^{1.21}(e/D_h)^{0.426}(p/e)^{2.94}[\exp(-0.71(\ln(p/e))^2)]$ vs $\phi/10$.

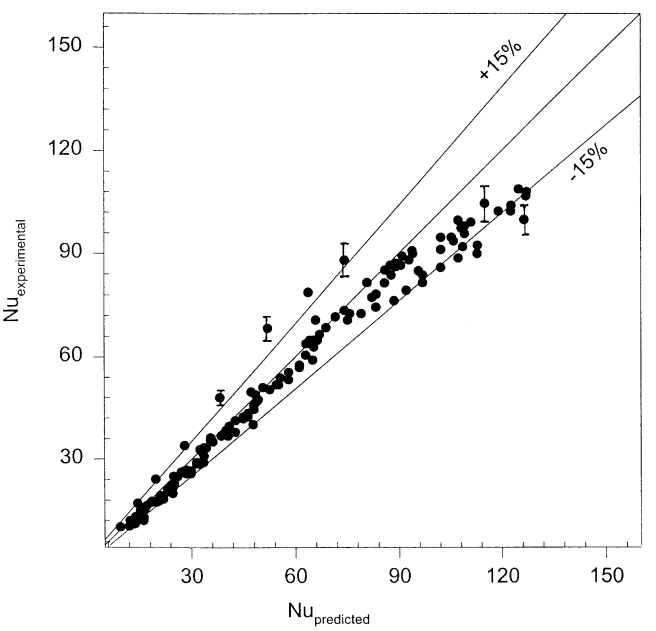

Fig. 26. Plot of predicted values vs experimental values of Nusselt number.

These values result in the following relationship for the Nusselt number:

$$Nu_r = 1.89\times10^{-4}(Re)^{1.21}(e/D_h)^{0.426}(p/e)^{2.94}[\exp(-0.71(\ln(p/e))^2)](\phi/10)^{-0.018}[\exp(-1.50(\ln(\phi/10))^2)] \quad (14)$$

8. Correlation for friction factor

A similar procedure has been employed to develop a correlation for the friction factor. The values of coefficient indicated in Figs 27 to 29 are:

$$A_{11}=0.15,\ B_{11}=4.11,\ C_{11}=12.57$$

The final correlation for friction factor can be written in the following form:Fig. 30

$$f_r = 12.44(Re)^{-0.18}(e/D_h)^{0.99}(p/e)^{-0.52}(\phi/10)^{0.49} \quad (15)$$

Figures 26 and 31 show the comparison between the experimental values of Nusselt number and friction factor and those predicted by the respective correlating Eq. (14) and Eq. (15). In Fig. 26 ninety percent of the data points lie within ±15% (146 out of 160). The standard deviation is ±9.1%. In Fig. 31 eighty-nine percent of data points lie within ±12% (143 out of 160). The standard deviation is ±8.2%.

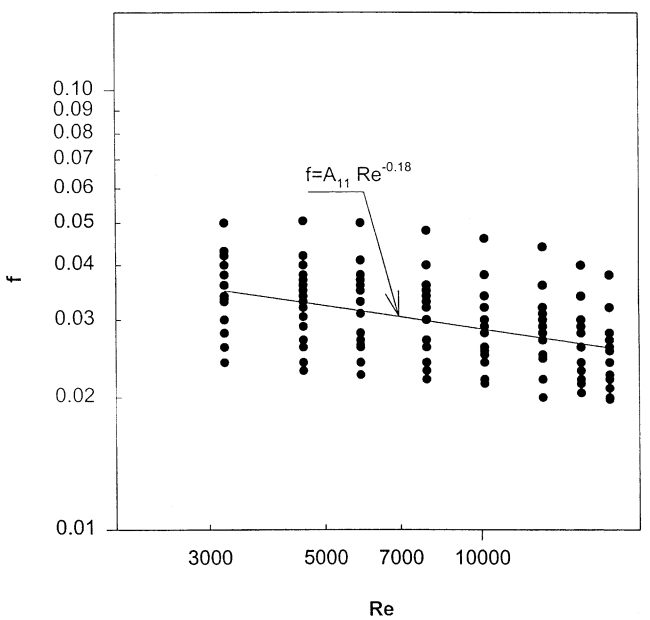

Fig. 27. Plot of f vs Re.

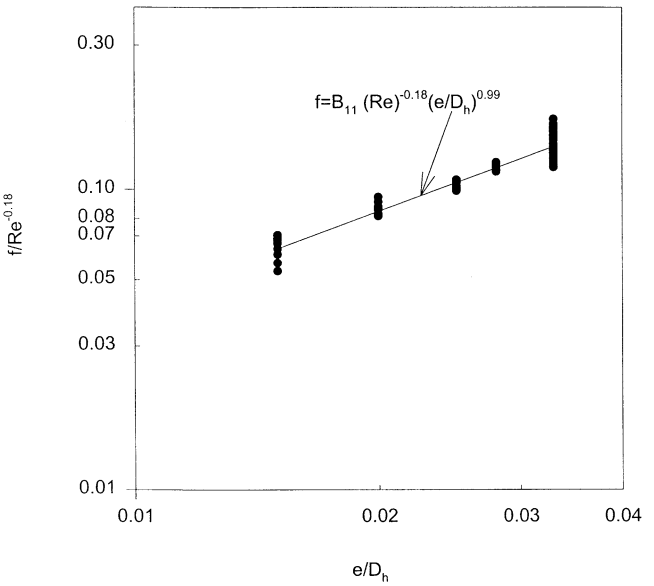

Fig. 28. Plot of $f/Re^{-0.18}$ vs e/D_h.

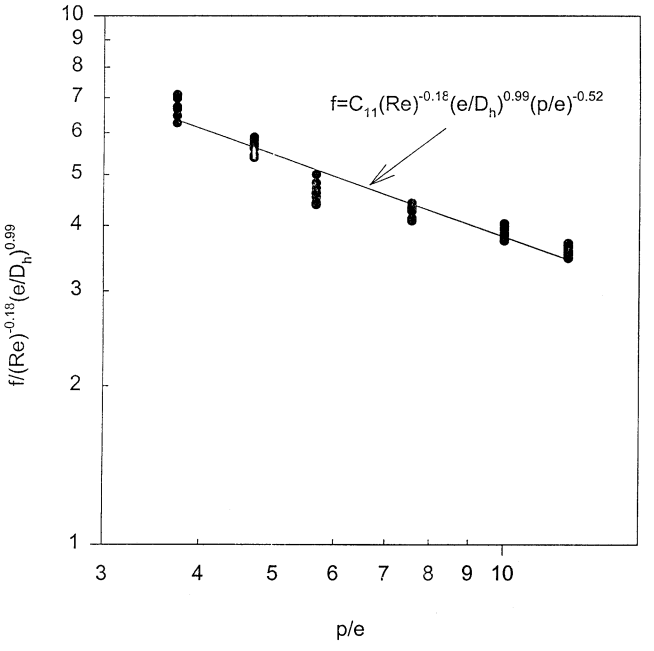

Fig. 29. Plot of $f/(Re)^{-0.18}(e/D_h)^{0.99}$ vs p/e.

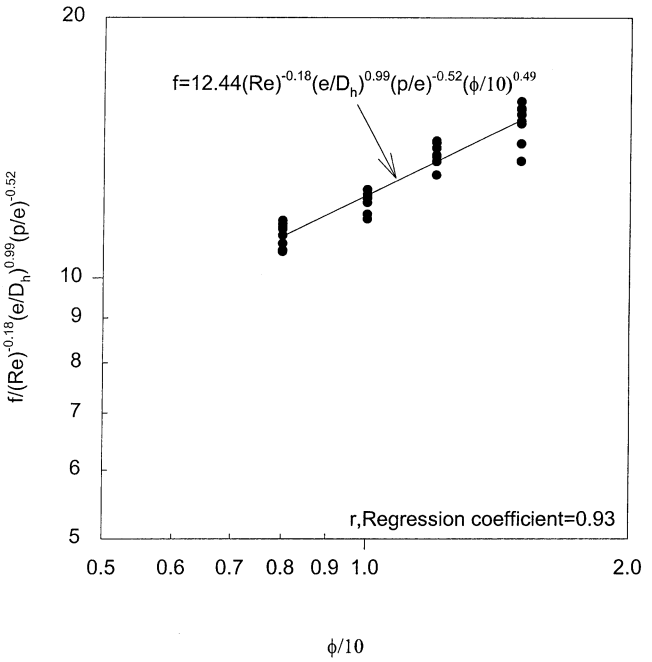

Fig. 30. Plot of $f/(Re)^{-0.18}(e/D_h)^{0.99}(p/e)^{-0.52}$ vs $\phi/10$.

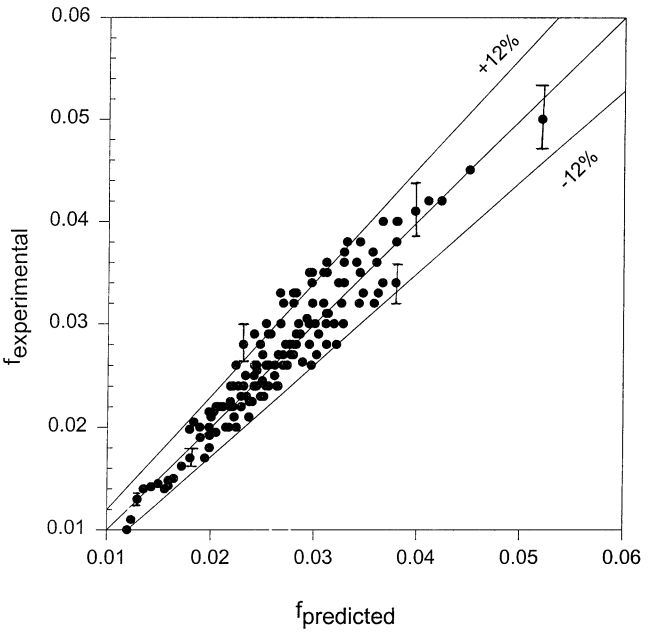

Fig. 31. Plot of predicted values vs experimental values of friction factor.

8.1. Conclusions

An experimental study of the flow of air in a rectangular duct with one roughened wall subjected to uniform heat flux has been performed, with the other three smooth walls being insulated. These conditions correspond to the flow in the duct of a solar air heater. The effect of relative roughness pitch, relative roughness height and wedge angle on the friction factor and heat transfer coefficient has been studied. The major conclusions are:

1. As compared to the smooth duct, the presence of ribs yields Nusselt number up to 2.4 times while the friction factor rises up to 5.3 times for the range of parameters investigated.
2. The maximum heat transfer occurs for a relative roughness pitch of about 7.57, while the friction factor keeps decreasing as the relative roughness pitch increases.
3. A maximum enhancement of heat transfer occurs at a wedge angle of about 10° while on either side of this wedge angle, Nusselt number decreases. The friction factor increases as the wedge angle increases.
4. Statistical correlations for Nusselt number and friction factor have been developed as functions of rib spacing, rib height, rib wedge angle, and Reynolds number. These correlations have been found to predict the values within the error limits of ±15% and ±12%.

References

[1] Nikuradse, J. Laws of flow in rough pipes. NACA, Technical Memorandum 1292. November 1970.
[2] Nunner, W. Heat transfer and pressure drop in rough tubes. VDI Forch 445-B 5-39 (1956); A.E.-R.E. Lib Trans. 786, 1958.
[3] Dippery DF, Sabersky RH. Heat and momentum transfer in smooth and rough tubes at various Prandtl number. Int J Heat Mass Transfer 1963;6:329–53.
[4] Ravigururajan TS, Bergles AE. General correlation for pressure drop and heat transfer for single-phase turbulent flow in internally ribbed tubes. Augmentation of heat transfer in energy systems. HTD52. New York: ASME, 1985:9-20.
[5] Han JC. Heat transfer and Friction in a channel with two opposite rib-roughened walls. Trans J Heat Transfer 1984;106:774–81.
[6] Webb RL, Eckert ERG, Goldstein RJ. Heat transfer and friction in tubes with repeated-rib roughness. Int J Heat Mass Transfer 1971;14:601–17.
[7] Han JC, Zhang YM. High performance heat transfer in ducts with parallel and broken ribs. Int J Heat Mass Transfer 1992;35:513–23.
[8] Liou TM, Hwang JJ. Effect of ridge shapes on turbulent heat transfer and friction in a rectangular channel. Int J Heat Mass Transfer 1993;36:933–40.
[9] Prasad BN, Saini JS. Effect of artificial roughness on heat transfer and friction factor in solar air heater. Solar Energy 1988;41(6):555–60.
[10] Gupta D. Investigations on fluid flow and heat transfer in solar air heater with roughened absorber. Ph.D. Thesis, U.O.R., Roorkee, India, 1993.
[11] Saini RP, Saini JS. Heat transfer and friction factor correlations for artificially roughened duct with expanded metal matrix as roughness elements. Int J Heat Mass Transfer 1997;40:973–86.

[12] Karwa R, Solanki SC, Saini JS. Heat transfer coefficient and friction factor correlations for the transitional flow regime in rib-roughened rectangular ducts. Int J Heat Mass Transfer 1999;42:1597–615.
[13] Williams F, Pirie MAM, Warburton C. Heat transfer from surfaces roughened by ribs. In: Bergles A, Webb RL, editors. ASME Symposium Volume: Augmentation of Convective Heat and Mass Transfer, 1970.
[14] Han JC, Park JS. Developing heat transfer in rectangular channels with rib-turbulators. Int J Heat Transfer 1988;31:183–95.
[15] Liou TM, Hwang JJ. Turbulent heat transfer augmentation and friction in periodic fully developed channel flow. J Heat Transfer 1992;114:56–63.
[16] ASHARE Standard 93-97. Method of testing to determine the thermal performance of solar collectors, 1977.
[17] Preobrazhensky VP. Measurement and Instrumentation in Heat Engineering [English translation], vol. 2. Moscow: Mir Publisher, 1980.
[18] Ehlinger AH. Flow of air and gases. In: Salisbury JK, editor. Kent's Mechanical Engineers Handbook, Power Volume. New York: Wiley, 1950:1.101.21.
[19] Holman JP. Experimental Methods for Engineers and Scientists. 2nd ed. McGraw-Hill, Inc, 1971.
[20] Bhatti MS, Shah RK. Turbulent and transition flow convective heat transfer. In: Kakac S, Shah RK, Aung W, editors. Handbook of Single-phase Convective Heat Transfer. New York: John Wiley and Sons, 1987.
[21] Kays W.M., Perkin H. Forced convection internal flow in ducts. In: Rohsenow W.M., Hartnett I.V., editors, Handbook of Heat Transfer. New York:McGraw-Hill.
[22] Kline SJ, McClintocK FA. Describe uncertainties in single sample experiments. Mech Engg 1953;75:3–8.
[23] Edwards F.J., Sheriff N. The Heat transfer and friction characteristics for forced convection air flow over a particular type of rough surface. International Developments in Heat Transfer. ASME, 1961:415-425.
[24] Emerson WH. Heat transfer in a duct in regions of separated flows. In: Proceedings of the Third International Heat Transfer Conference, 1966:267–75.